Half-skyrmion and vortex-antivortex pairs in spinor condensates

Yu-Xin Hu (胡渝鑫),[1,2] Christian Miniatura,[1,2,3,4,5] and Benoît Grémaud[1,2,3,6]

[1]*Centre for Quantum Technologies, National University of Singapore, 3 Science Drive 2, Singapore 117543, Singapore*

[2]*MajuLab, CNRS-UNS-NUS-NTU International Joint Research Unit UMI 3654, Singapore*

[3]*Department of Physics, National University of Singapore, 2 Science Drive 3, Singapore 117542, Singapore*

[4]*Institut Non Linéaire de Nice, UMR 7335, UNS, CNRS; 1361 route des Lucioles, 06560 Valbonne, France*

[5]*Institute of Advanced Studies, Nanyang Technological University, 60 Nanyang View, Singapore 639673, Singapore*

[6]*Laboratoire Kastler Brossel, Ecole Normale Supérieure CNRS, UPMC; 4 Place Jussieu, 75005 Paris, France*

(Received 11 November 2014; revised manuscript received 31 March 2015; published 17 September 2015)

We propose a simple experimental scheme to generate spin textures in the ground state of interacting ultracold bosonic atoms loaded in a two-dimensional harmonic trap. Our scheme is based on two copropagating Laguerre-Gauss laser beams illuminating the atoms and coupling two of their internal ground state Zeeman sublevels. Using a Gross-Pitaevskii description, we show that the ground state of the atomic system has different topological properties depending on the interaction strength and the laser beam intensity. A half-skyrmion state develops at low interactions while a vortex-antivortex pair develops at large interactions.

DOI: 10.1103/PhysRevA.92.033615 PACS number(s): 67.85.Fg, 03.75.Lm, 37.10.Vz

I. INTRODUCTION

Because of their ability to materialize abstract theoretical models into carefully designed and controlled experiments, ultracold quantum gases have successfully pervaded many diverse fields of physics ranging from lattice and spin systems, quantum information, quantum simulators, to gauge fields and Anderson localization to cite a few [1]. This is particularly true in the condensed-matter realm where they became a key player in many-body physics as exemplified by the first observation of the Mott-superfluid transition [2–4].

In recent years, the physics of the quantum Hall effects has become one important focus of the ultracold atoms community. Because atoms are neutral, one needed effective schemes to mimic the action of a magnetic field. A first idea was to set quantum gases into rapid rotation [5] but it faded away because more promising alternatives using light-atom coupling were quickly proposed and experimentally studied [6–12]. A large variety of Hamiltonians, including non-Abelian ones, either in lattices or in the bulk [13–16], have been now proposed to mimic magnetic field configurations like artificial Dirac monopoles [17,18], spin-orbit (SO) coupling [19–21] or topological phases [22,23]. For instance, for atoms loaded in a square optical lattice, SO coupling leads to highly nontrivial properties like ground states breaking time reversal invariance and/or magnetic textures with topological properties, like a skyrmion crystal [24–26]. Such skyrmionic structures have been experimentally observed in excitations of cold atomic gases [27], but not yet in the ground state. From a theorerical point of view, some papers have proposed to generate these topological configurations with cold atomic gases either in transient excitations, which decay eventually to a nontopological configuration [28], or directly in the ground state [29,30]. However the actual experimental implementation of the latter proposal remains quite challenging.

In the present paper, we provide a rather simple experimental setup to generate spin textures in the ground state of interacting ultracold bosonic atoms loaded in a two-dimensional harmonic trap. Our scheme is based on two copropagating Laguerre-Gauss laser beams illuminating the atoms and coupling two of their internal ground state Zeeman sublevels. At the mean-field level, i.e., using a Gross-Pitaevskii description, we show that the ground state of the atomic system has different topological properties depending on the interaction strength and the laser beam intensity. A half-skyrmion state, also known as a Mermin-Ho vortex [31], develops at low interactions while a meron pair develops at large interactions.

In the following, we first introduce our model and its effective Hamiltonian, then we briefly present the essential properties of the single particle states. Next, we analyze the topological properties of the ground state in the weak interaction limit. Finally, we show that at large interactions there is a transition to a ground state made of a vortex-antivortex pair separated by a finite distance. The separation between the two opposite vortices vanishes at the transition and increases with the interaction.

II. MODEL HAMILTONIAN

A. Experimental Setup

We consider here bosonic ultracold atoms with 3 internal ground state levels, for instance the $F = 1$ states of ^{87}Rb. We assume the atoms are harmonically trapped in the two-dimensional plane (x,y) and tightly confined in the third direction z (chosen as the quantization axis) so that the atomic dynamics is effectively two dimensional. The atoms are further subjected to a static magnetic field along z splitting the Zeeman degeneracy and are illuminated by two far-detuned laser beams (blue detuning) copropagating along z with opposite circular polarizations. These two laser beams create a resonant Raman coupling between the Zeeman sublevels $m_F = \pm 1$; see Fig. 1 (Λ scheme). In the rotating-wave approximation, and after adiabatic elimination of the excited state, the effective 2×2 Hamiltonian describing the dynamics in the (x,y) plane for the $m_F = \pm 1$ ground state manifold reads [6,7,13,16,27,32–36] (see the Appendix):

$$H_e + \left(\frac{p^2}{2M} + \frac{1}{2}M\omega^2 r^2\right)\mathbb{1} + \frac{1}{4\Delta}\begin{pmatrix} |\Omega_1|^2 & \Omega_2\Omega_1^* \\ \Omega_1\Omega_2^* & |\Omega_2|^2 \end{pmatrix}, \quad (1)$$

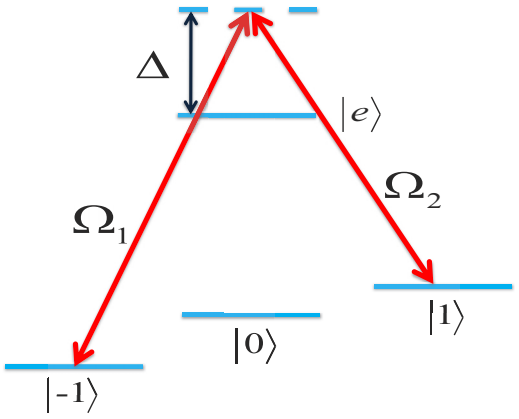

FIG. 1. (Color online) The two lowest single-particle energies (in units of $\hbar\omega$) as a function of the dimensionless Rabi frequency Ω. The horizontal red dashed line corresponds to the non degenerate spinor state $\underline{\phi_0}$ where $g_0 = -f_0$, see text. The black solid line corresponds to the degenerate spinor states $\underline{\phi_1}$ and $\mathcal{T}\underline{\phi_1}$, see text.The two energy branches cross at the critical value $\Omega_c \simeq 3.35$.

where M is the mass of the atoms, ω the harmonic trapping frequency and $r = \sqrt{x^2 + y^2}$ the radial distance in the plane and where we have used the pseudospin representation $|\downarrow\rangle \equiv |m_F = -1\rangle$ and $|\uparrow\rangle \equiv |m_F = 1\rangle$. In the specific case of Laguerre-Gauss beams [27,37] with equal (real) strength Ω_0 and carrying opposite orbital angular momentum $\pm\hbar$, the respective Rabi frequencies read:

$$\Omega_1 = \Omega_0 \frac{r}{R} e^{i(kz+\varphi)}, \quad \Omega_2 = \Omega_0 \frac{r}{R} e^{i(kz-\varphi)}, \tag{2}$$

where R is the size of the "doughnut" core, k the laser wave number, and φ the polar angle of vector $\mathbf{r} = (x, y)$. We assume here that the transverse size of the laser beams is much larger than the atomic cloud.

In the following, we use the harmonic oscillator quantum of energy $\hbar\omega$, the harmonic length $a_{ho} = \sqrt{\hbar/M\omega}$, and $\hbar/a_{ho}$ as energy, space and momentum units. We also denote the usual Pauli spin matrices by σ_x, σ_y, and σ_z. The dimensionless single-particle effective Hamiltonian then reads:

$$H_0 = \left(\tfrac{1}{2}\mathbf{p}^2 + \tfrac{1}{2}r^2\right)\mathbb{1} + \tfrac{1}{2}\Omega^2 r^2 \begin{pmatrix} 1 & e^{-2i\varphi} \\ e^{2i\varphi} & 1 \end{pmatrix}, \tag{3}$$

with $\Omega^2 = \Omega_0^2/(2M\omega^2 R^2 \Delta)$ and where $\mathbf{p} = -i\nabla$. As easily checked, this Hamiltonian is invariant under a *combined* space and spin rotation, namely, $H_0 = R(\varphi_0) H_0 R^\dagger(\varphi_0)$ where $R(\varphi_0) = e^{i\varphi_0(\hat{L}_z + \sigma_z)}$ is the operator associated to a rotation by an angle φ_0 around z both in coordinate and spin space. Here $L_z = -i\partial/\partial\varphi$ is the orbital angular momentum operator around z. Applying the unitary transformation $U(\varphi) = e^{i\varphi\sigma_z}$, one gets the unitary-equivalent Hamiltonian $\tilde{H}_0 = U H_0 U^\dagger$ with

$$\tilde{H}_0 = \frac{1}{2}\left(\mathbf{p}\mathbb{1} + \frac{\hat{e}_\varphi}{r}\sigma_z\right)^2 + \frac{1}{2}(1 + \Omega^2) r^2 \mathbb{1} + \frac{1}{2}\Omega^2 r^2 \sigma_x. \tag{4}$$

In this new gauge, $\tilde{H}_0$ can be viewed as the Hamiltonian of a particle subjected to the artificial gauge potential $\mathbf{A} = -\frac{1}{r}\hat{e}_\varphi\,\sigma_z$ [16] associated to two infinite strings carrying opposite magnetic fluxes $\Phi = \pm 2\pi$, one along the positive z axis, the other one along the negative z axis. The corresponding magnetic field is simply given by $\mathbf{B} = 2\pi\delta(\mathbf{r})\hat{e}_z\,\sigma_z$.

B. Single-particle eigenstates

Since H_0 is invariant under a combined spin and space rotation, its spinor eigenstates in the pseudospin basis ($|\downarrow\rangle$, $|\uparrow\rangle$) have the general structure:

$$\underline{\phi_m}(\boldsymbol{r}) = \begin{pmatrix} \phi_{m\uparrow}(\boldsymbol{r}) \\ \phi_{m\downarrow}(\boldsymbol{r}) \end{pmatrix} = \begin{pmatrix} f_m(r) e^{-i\varphi} \\ g_m(r) e^{i\varphi} \end{pmatrix} \frac{e^{im\varphi}}{\sqrt{2\pi}}, \tag{5}$$

where m is an integer. Inspection of the coupled Schrödinger equations for the eigenstates shows that both radial functions $f_m(r)$ and $g_m(r)$ can be chosen real. H_0 is also invariant under the operator $\mathcal{T} = \sigma_x \mathcal{C}$, $H_0 = \mathcal{T} H_0 \mathcal{T}^{-1}$, where $\mathcal{C}$ represent complex conjugation. This implies that both $\underline{\phi_m}(\mathbf{r})$ and $\mathcal{T}\underline{\phi_m}(\mathbf{r})$ are eigenstates of H_0 with the same eigenenergy $\epsilon_{|m|}(\Omega)$. Since $\mathcal{T}\underline{\phi_m}(\mathbf{r}) = \pm\underline{\phi_{-m}}(\mathbf{r})$, we have $g_m = \pm f_{-m}$ and we can restrict the analysis to the $m \geqslant 0$ sector. Noting that $\underline{\phi_m}(\mathbf{r})$ and $\mathcal{T}\underline{\phi_m}(\mathbf{r})$ are orthogonal spinors when $m \neq 0$, we conclude that their corresponding eigenenergy is doubly degenerate when $\Omega > 0$.

Figure 2 displays the two lowest eigenenergies of H_0 as a function of the dimensionless Rabi frequency Ω. Below $\Omega_c \simeq 3.35$, the ground state manifold is doubly degenerate and is spanned by the two spinor states $\underline{\phi_1}(\mathbf{r})$ and $\mathcal{T}\underline{\phi_1}(\mathbf{r})$. We find that $f_1(r)$ reaches a finite value at the origin $r = 0$ while $g_1(r)$ vanishes. This means that the spin-down component of $\underline{\phi_1}(\mathbf{r})$, $g_1(r)\exp(2i\varphi)$, depicts a vortex with vorticity equal to 2 while the spin-up component of $\mathcal{T}\underline{\phi_1}(\mathbf{r})$, $g_1(r)\exp(-2i\varphi)$, depicts the opposite vortex. A convenient parametrization of the spinor proves to be $\underline{\phi_1}(\mathbf{r}) = \sqrt{n_1(r)}\,\underline{\chi_1}(\mathbf{r})$ where

$$\underline{\chi_1}(\mathbf{r}) = \begin{pmatrix} \chi_{1\uparrow}(\mathbf{r}) \\ \chi_{1\downarrow}(\mathbf{r}) \end{pmatrix} = \begin{pmatrix} -\cos\frac{\beta(r)}{2} \\ e^{i2\varphi}\sin\frac{\beta(r)}{2} \end{pmatrix} \tag{6}$$

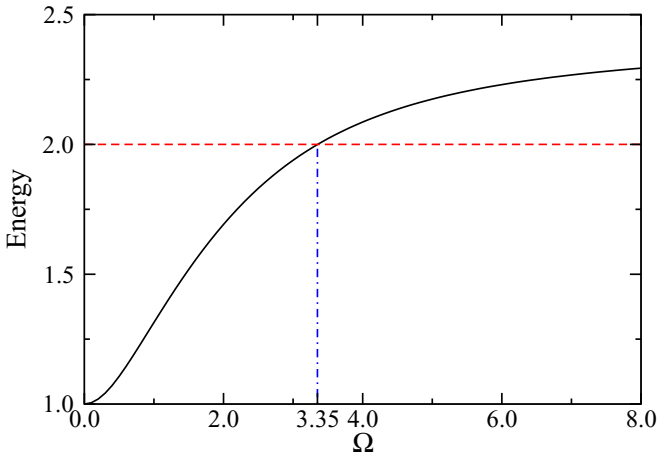

FIG. 2. (Color online) The two lowest single-particle energies (in units of $\hbar\omega$) as a function of the dimensionless Rabi frequency Ω. The horizontal points (in red) correspond to the nondegenerate spinor state $\underline{\phi_0}$ where $g_0 = -f_0$; see text. The star symbols (in blue) correspond to the degenerate spinor states $\underline{\phi_1}$ and $\mathcal{T}\underline{\phi_1}$; see text. The two energy branches cross at the critical value $\Omega_c \simeq 3.35$.

and $n_1(r) = f_1^2(r) + g_1^2(r)$ is the total density. As $n_1(r)$ is finite at the origin and $g_1(r)$ vanishes, we must have $\beta(0) = 0$. We also find $\beta(\infty) = \pi/2$ corresponding to $n_\uparrow = n_\downarrow$ at large distances. A configuration satisfying such boundary conditions is known as a Mermin-Ho vortex [31], also called a half-skyrmion since one has $\beta(\infty) = \pi$ for a "full" skyrmion. The local spin texture is defined by

$$\begin{aligned} \boldsymbol{S}(\mathbf{r}) &= \underline{\chi_1}(\mathbf{r})^\dagger \boldsymbol{\sigma}\, \underline{\chi_1}(\mathbf{r}) \\ &= -\sin\beta(r)(\cos 2\varphi\, \hat{e}_x + \sin 2\varphi\, \hat{e}_y) + \cos\beta(r)\, \hat{e}_z, \end{aligned} \quad (7)$$

with modulus $|\boldsymbol{S}(\mathbf{r})| = 1$. It characterizes a two-dimensional (2D) Skyrmion with topological charge [38]

$$Q = \int d^2\mathbf{r}\, q(\mathbf{r}) = \int d^2\mathbf{r}\, \epsilon^{ij}\, \frac{\boldsymbol{S}\cdot(\partial_i \boldsymbol{S}\times\partial_j \boldsymbol{S})}{8\pi}, \quad (8)$$

where $i,j = x,y$ and where ϵ^{ij} is the antisymmetric tensor. Using the parametrization given by Eq. (7), the topological charge density is simply

$$q(\boldsymbol{r}) = \epsilon^{ij}\, \frac{\boldsymbol{S}\cdot(\partial_i \boldsymbol{S}\times\partial_j \boldsymbol{S})}{8\pi} = -\frac{1}{2\pi r}\frac{d\cos\beta(r)}{dr}. \quad (9)$$

We thus find that, for $\Omega < \Omega_c$, the topological properties of the ground state spin texture of our noninteracting system are described by a Mermin-Ho vortex with unit topological charge $Q = \cos\beta(0) - \cos\beta(\infty) = 1$.

Above Ω_c, the ground state manifold is nondegenerate and the eigenstate is now the spinor $\underline{\phi_0}(\mathbf{r})$ where $g_0(r) = -f_0(r)$. Since $f_0(r)$ vanishes at the origin, we see that the two spin components, $\phi_{0\uparrow}(\mathbf{r}) = f_0(r)e^{-i\varphi}$ and $\phi_{0\downarrow}(\mathbf{r}) = -f_0(r)e^{+i\varphi}$, describe opposite vortices with unit vorticity.

III. INTERACTING BOSONS

We assume here that the atoms in the $m_F = \pm 1$ Zeeman states interact through a fully $SU(2)$-symmetric interaction and are not coupled to the $m_F = 0$ state. The corresponding second-quantized Hamiltonian reads

$$H_{\rm int} = \frac{g}{2}\int d^2\boldsymbol{r}\, \Psi_a^\dagger \Psi_b^\dagger \Psi_b \Psi_a, \quad (10)$$

where g is the dimensionless interaction strength and where summation over the dummy pseudospin indices a and b is understood. Here $\Psi_a^\dagger$ and Ψ_a stand for the creation and destruction operators of a particle at point $\mathbf{r}$ in spin component $a = \uparrow,\downarrow$. They satisfy the usual bosonic commutation relations $[\Psi_a, \Psi_b^\dagger] = \delta_{ab}$. We next assume that, in the zero temperature limit, all the bosons condense into a single spinor coherent state $\underline{\Phi}(\mathbf{r})$ with spin components $\Phi_\uparrow(\boldsymbol{r})$ and $\Phi_\downarrow(\boldsymbol{r})$, and we describe the interacting system within a mean-field approach. The Gross-Pitaevskii (GP) energy functional reads

$$E[g, \underline{\Phi}(\mathbf{r})] = \int d^2\mathbf{r}\left[\underline{\Phi}^\dagger H_0 \underline{\Phi} + \frac{g}{2}(\underline{\Phi}^\dagger\underline{\Phi})^2\right], \quad (11)$$

where $\underline{\Phi}^\dagger\underline{\Phi} = n(\mathbf{r}) = n_\uparrow(\mathbf{r}) + n_\downarrow(\mathbf{r}) = |\Phi_\uparrow(\mathbf{r})|^2 + |\Phi_\downarrow(\mathbf{r})|^2$ is subjected to the normalization condition $\int d^2\boldsymbol{r}\, n(\mathbf{r}) = 1$.

A. Weak interaction regime

1. Case $\Omega < \Omega_c$

In the limit $g \to 0$, only states with an energy separation $|\delta E| \simeq g$ or lower are efficiently coupled. Therefore, in first approximation, we expect the ground state $\underline{\phi_g}(\boldsymbol{r})$ to belong to the single-particle ground state manifold. We thus look for the simple ansatz $\underline{\phi_g}(\boldsymbol{r}) = \alpha\, \underline{\phi_1}(\boldsymbol{r}) + \beta\, \mathcal{T}\underline{\phi_1}(\boldsymbol{r})$, where the minimization parameters α and β are two constant complex numbers satisfying $|\alpha|^2 + |\beta|^2 = 1$. It is easy to check that the corresponding GP energy functional is always larger than the one computed with $\underline{\phi_1}(\boldsymbol{r})$ alone [which is also equal to that computed with $\mathcal{T}\underline{\phi_1}(\boldsymbol{r})$ alone]. This means that, when $g \to 0$, the $\mathcal{T}$ symmetry is spontaneously broken: $\underline{\phi_g}(\boldsymbol{r}) = \underline{\phi_1}(\boldsymbol{r})$ ($\alpha = 1$) or $\underline{\phi_g}(\boldsymbol{r}) = \mathcal{T}\underline{\phi_1}(\boldsymbol{r})$ ($\beta = 1$). The spin texture associated to this weakly interacting GP ground state is a Mermin-Ho vortex with unit topological charge. We have numerically computed the exact GP ground state and checked that the previous ansatz provides a qualitatively correct picture at small values of the interaction strength g. For instance, the density profiles $n(\mathbf{r})$, $n_\uparrow(\mathbf{r})$, $n_\downarrow(\mathbf{r})$ and the topological charge density $q(\mathbf{r})$ of the exact GP spinor ground state are displayed in Fig. 3 for $g = 0.1$ and $\Omega = 2$. One can clearly see that $n_\uparrow$ remains finite whereas $n_\downarrow$ vanishes at the center of the trap; in addition, the ground state depicts a nontrivial topological charge density, with a total topological charge $Q = \int d^2\boldsymbol{r}\, q(\boldsymbol{r}) = 1$. This emphasizes that the GP ground state has the same topology as a Mermin-Ho vortex with unit topological charge.

Starting from one of the single-particle ground states selected in the limit $g \to 0$, we now increase the interaction strength g. Spinor $\underline{\phi_0}$ can no longer be ignored now, especially when Ω is close to Ω_c and $\underline{\phi_1}$, $\mathcal{T}\underline{\phi_1}(\boldsymbol{r})$, and $\underline{\phi_0}$ are almost degenerate. An updated ansatz simply reads $\underline{\phi_g}(\boldsymbol{r}) = \alpha\underline{\phi_1}(\boldsymbol{r}) + \beta\mathcal{T}\underline{\phi_1}(\boldsymbol{r}) + \gamma\underline{\phi_0}(\boldsymbol{r})$ with constant complex parameters satisfying $|\alpha|^2 + |\beta|^2 + |\gamma|^2 = 1$. We find that there exists a critical interaction strength $g_c(\Omega)$ such that $\underline{\phi_g} = \underline{\phi_1}$ (or $\mathcal{T}\underline{\phi_1}$) when $g < g_c$ and $\underline{\phi_g} = \underline{\phi_0}$ when $g > g_c$. The reason for this phase transition is that the spinor $\underline{\phi_0}$ carries less interaction energy than $\underline{\phi_1}$ and $\mathcal{T}\underline{\phi_1}$. Indeed its total density

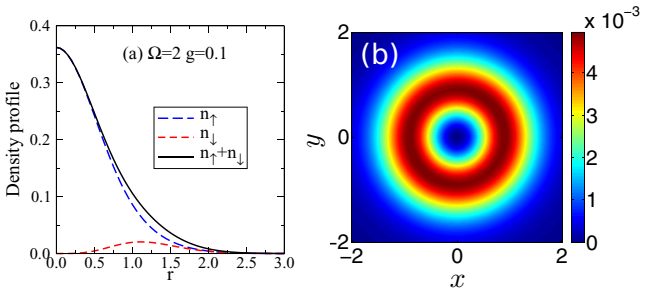

FIG. 3. (Color online) (a) Radial density profiles of the GP spinor ground state for an interaction strength $g = 0.1$ and a potential energy $\Omega = 2$, obtained from an exact numerical calculation. (b) Corresponding topological charge density $q(\boldsymbol{r})$; see Eqs. (7) and (9). Only the spin-down density $n_\downarrow(r)$ is vanishing at the origin, indicating that the spin-down component hosts a vortex with a vorticity equal to 2. The total topological charge is $Q = \int d^2\boldsymbol{r}\, q(\boldsymbol{r}) = 1$. The length unit is set by $a_{ho} = \sqrt{\hbar/M\omega}$.

$n_0(r)$ is vanishing at the trap center whereas the total density $n_1(r)$ is maximum there. At the mean-field level, this transition is first order since the states have different vorticities.

For each Ω, the critical interaction strength g_c is obtained by equating the two energy functionals Eq. (11) obtained in each symmetry sector m ($m = 0,1$). It amounts to solving the functional equation

$$g_c = \frac{\int d^2\mathbf{r}\,[\underline{\Phi}_1^+ H_0 \underline{\Phi}_1 - \underline{\Phi}_0^+ H_0 \underline{\Phi}_0]}{V_0 - V_1} \equiv F[g_c]. \qquad (12)$$

Here, $\underline{\Phi}_m$ is the GP ground state obtained in the symmetry sector m at the interaction strength g_c and $V_m = \frac{1}{2}\int d^2\mathbf{r}\,(\underline{\Phi}_m^+ \underline{\Phi}_m)^2$. In practice, $\underline{\Phi}_m$ is obtained by running the imaginary-time evolution algorithm, starting from the single-particle states $\underline{\phi}_m$. The invariance of the GP equation under a combined spin and space rotation ensures that the imaginary-time evolved state always remains inside the chosen symmetry sector. We solve Eq. (12) iteratively by starting from $g_c^{(0)} = 0$. The first estimate of the critical interaction $g_c^{(1)} = F[0]$ is thus simply obtained by computing the energy functionals with the single-particle ground states. The result is shown in Fig. 4 (dashed line). One may notice that this first-iteration prediction for g_c is not really weak unless Ω is very close to Ω_c. This means that approximating the true GP ground state by one of the single-particle states becomes questionable. A more accurate estimate is thus obtained by doing a second iteration step $g_c^{(2)} = F[g_c^{(1)}]$. The result is shown in Fig. 4 (continuous line) and is in very good agreement with the exact value for g_c (star symbols) obtained by finding, for each Ω, the global minimum of the GP energy functional as a function of g and monitoring the symmetry and topological properties of the corresponding ground states.

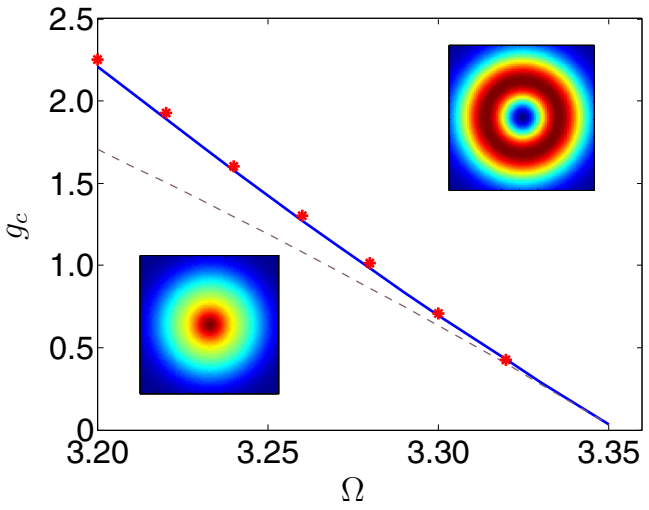

FIG. 4. (Color online) Critical value g_c for the transition from the $m = 1$ to the $m = 0$ spinor states as a function of Ω. Dashed line: prediction obtained by comparing the GP energies computed with the single-particle spinors. The agreement is fair only for Ω very close to Ω_c. Continuous line: prediction obtained by comparing the GP energies computed with the GP ground states found, in each sector $m = 0$ or $m = 1$, at the interaction strength given by the dashed line. Star symbols: prediction obtained by minimizing the GP energy functional. As one can see the agreement with the continuous line is very good. The inset shows the corresponding spin-up density $n_\uparrow(\mathbf{r})$ below and above the critical line. The length unit is set by $a_{ho} = \sqrt{\hbar/M\omega}$.

2. $\Omega > \Omega_c$

In this case, the single-particle ground state is $\underline{\phi}_0$ and it qualitatively describes the properties of the GP ground state in the weakly interacting regime. This is confirmed by our exact numerical results which show that the GP ground state indeed hosts a vortex in each of its components, but with opposite vorticity.

B. Strong interaction regime

In the strong interacting regime, higher single-particle states are coupled and no simple ansatz can be made. In this case we obtain the interacting ground state $\underline{\phi}_g$ by direct minimization of the GP energy functional Eq. (11). This is achieved by imaginary-time evolution of the corresponding GP equation. Figure 5 shows the ground state density of the up and down components and their relative phase $(\theta_\downarrow - \theta_\uparrow)$ when $g = 100$ and $\Omega = 4$. As one can see, each component density vanishes at an off-centered location, at which the other component reaches its maximum, reducing thereby the overlapping area between the two components and therefore their interaction energy. The two points at which the densities vanish are located at symmetric positions $x = \pm x_m$ with respect to the center of the trap. In addition, the relative phase between the two components exhibits two clear 2π jumps along the two segments $]-\infty,-x_m]$ and $[x_m,+\infty[$ on axis x.

To gain further insight, we introduce again the pseudospin representation and decompose the GP spinor components as

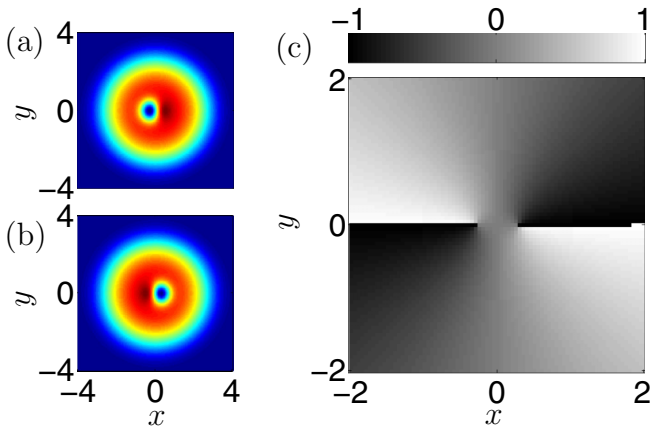

FIG. 5. (Color online) Density profile of (a) the spin-down component and (b) the spin-up component of the GP ground state spinor at $\Omega = 4$ and $g = 100$. They describe a meron pair: each component hosts a vortex, the two vortices are separated by a distance $2x_m$ and have opposite vorticities. The relative phase $(\theta_\downarrow - \theta_\uparrow)$ (in units of π) is shown in (c). There are two clear 2π jumps on each side of the meron pair, emphasizing that the vortex charge is ± 1. One may note that the total relative phase accumulated along a loop encircling the two vortices is 4π, a situation that differs from the usual meron pair [29] where the phase jump happens when one crosses the line connecting the vortex centers. The length unit is set by $a_{ho} = \sqrt{\hbar/M\omega}$.

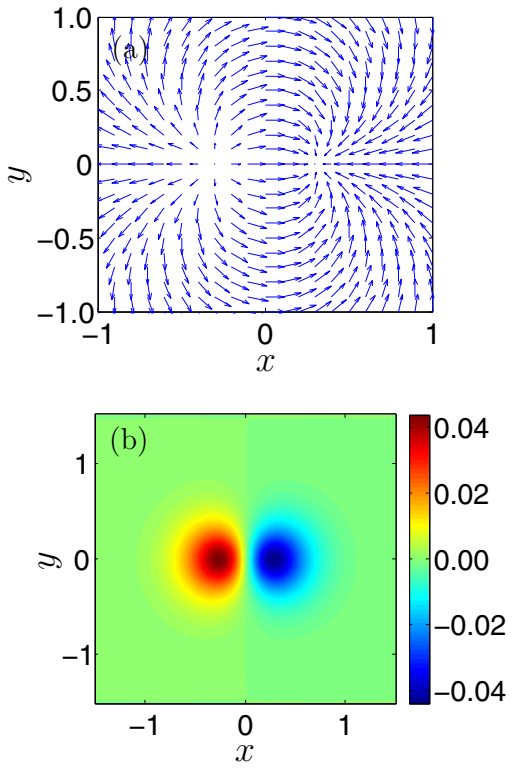

FIG. 6. (Color online) Topological properties of the GP ground state for $\Omega = 4$ and $g = 100$. (a) Spin texture components (S_x, S_y) in the plane (x, y). Around the left vortex $\boldsymbol{S} = -\mathbf{e}_z$, the texture corresponds to $(S_x, S_y) \propto (\delta x, \delta y)$, whereas it corresponds to $(S_x, S_y) \propto (-\delta x, -\delta y)$ around the right vortex $\boldsymbol{S} = \mathbf{e}_z$; see text. (b) The corresponding topological charge density; see Eqs. (8) and (18). The distribution is odd with respect to the x coordinate, which emphasizes the creation of a vortex-antivortex pair with vanishing total topological charge. The length unit is set by $a_{ho} = \sqrt{\hbar/M\omega}$.

$\phi_{g,a} = \sqrt{n}\,\chi_a$ with $\chi_a = |\chi_a| e^{i\theta_a}$ $(a = \uparrow, \downarrow)$. The total density is $n = |\phi_\uparrow|^2 + |\phi_\downarrow|^2$ and the spinor $\underline{\chi}$ thus satisfies $|\chi_\uparrow|^2 + |\chi_\downarrow|^2 = 1$. The corresponding local spin texture $\boldsymbol{S} = \underline{\chi}^\dagger \boldsymbol{\sigma}\, \underline{\chi}$ reads

$$\begin{aligned} S_x &= 2|\chi_\uparrow||\chi_\downarrow| \cos(\theta_\downarrow - \theta_\uparrow), \\ S_y &= 2|\chi_\uparrow||\chi_\downarrow| \sin(\theta_\downarrow - \theta_\uparrow), \\ S_z &= |\chi_\uparrow|^2 - |\chi_\downarrow|^2. \end{aligned} \tag{13}$$

and has unit modulus $|\boldsymbol{S}| = 1$. This local spin is parallel to axis z, namely, $\boldsymbol{S} = \hat{e}_z$ (respectively, $\boldsymbol{S} = -\hat{e}_z$) at space points where $n_\downarrow$ (respectively, $n_\uparrow$) vanishes. The relative phase $(\theta_\downarrow - \theta_\uparrow)$ is undefined at these two points and they correspond to a vortex-antivortex pair. These properties appear clearly in Fig. 6(a) where the spin components (S_x, S_y) are plotted in the plane (x, y). Writing $\mathbf{r} = (-x_m + \delta x, \delta y)$, we find $(S_x, S_y) \propto (\delta x, \delta y)$ around the left vortex $\boldsymbol{S} = -\hat{e}_z$. By the same token, writing $\mathbf{r} = (x_m + \delta x, \delta y)$, we find $(S_x, S_y) \propto (-\delta x, -\delta y)$ around the right vortex $\boldsymbol{S} = +\mathbf{e}_z$. The topological charge density, computed with Eq. (8), is displayed in Fig. 6. It emphasizes that the GP ground state spinor depicts two vortices with opposite vorticity (with respect to S_z), such that the total topological charge vanishes.

In the pseudospin representation [30,39], the GP energy functional reads

$$\begin{aligned} E = \int d^2 r \Big[&\frac{1}{2}(\boldsymbol{\nabla}\sqrt{n})^2 + \frac{n}{8}(\boldsymbol{\nabla}\boldsymbol{S})^2 + \frac{n}{2}\boldsymbol{v}_e^2 + \frac{r^2}{2} n \\ &+ \frac{1}{2}\Omega^2 r^2 (I + S_x \cos 2\varphi + S_y \sin 2\varphi) + \frac{g}{2} n^2 \Big], \end{aligned} \tag{14}$$

where

$$(\boldsymbol{\nabla}\boldsymbol{S})^2 \stackrel{\text{def}}{=} (\boldsymbol{\nabla} S_x)^2 + (\boldsymbol{\nabla} S_y)^2 + (\boldsymbol{\nabla} S_z)^2. \tag{15}$$

The effective velocity field is given by [30,39]

$$\boldsymbol{v}_e = \frac{1}{2}\left[\boldsymbol{\nabla}\Theta + \frac{S_z (S_y \boldsymbol{\nabla} S_x - S_x \boldsymbol{\nabla} S_y)}{S_x^2 + S_y^2} \right], \tag{16}$$

and depends on the gradient of the total phase $\Theta = \theta_\uparrow + \theta_\downarrow$ and of the pseudospin. In analogy with the meron pair solution discussed in [29,40,41], we parametrize the spin texture as follows:

$$\begin{aligned} S_x &= \frac{-r^2 \cos 2\varphi + \lambda^2 e^{-\alpha r^2}}{r^2 + \lambda^2 e^{-\alpha r^2}}, \quad S_y = \frac{-r^2 \sin 2\varphi}{r^2 + \lambda^2 e^{-\alpha r^2}}, \\ S_z &= -\frac{2\lambda e^{-\alpha r^2/2}\, r \cos\varphi}{r^2 + \lambda^2 e^{-\alpha r^2}}. \end{aligned} \tag{17}$$

The usual meron pair parametrization is obtained for $\alpha = 0$. The corresponding topological charge density is

$$q(\boldsymbol{r}) = -\frac{\mu\, x}{\pi(r^2 + \mu^2)^2} - \alpha \frac{\mu\, x r^2}{\pi(r^2 + \mu^2)^2}, \tag{18}$$

where $\mu = \lambda e^{-\alpha r^2/2}$. The vortex-antivortex nature of the meron pair results in a topological density $q(\boldsymbol{r})$ which is an odd function of coordinate x; see Fig. 6(b). As a consequence, the total topological charge is $Q = \int d\boldsymbol{r}\, q(\boldsymbol{r}) = 0$.

The spin texture Eq. (17) corresponds to the GP spinor condensate:

$$\phi_\uparrow = \sqrt{\frac{n}{2}}\, \frac{\mu - r e^{-i\varphi}}{\sqrt{r^2 + \mu^2}}, \quad \phi_\downarrow = \sqrt{\frac{n}{2}}\, \frac{\mu + r e^{i\varphi}}{\sqrt{r^2 + \mu^2}}. \tag{19}$$

The meron pair is polarized along axis x due to the σ_x term in Eq. (4) which describes an effective magnetic field along x. The locations of the two vortex cores are determined by the two extremas of S_z. They are found at $(\pm x_m, 0)$ where [29]

$$x_m^2 = \lambda^2 e^{-\alpha x_m^2}. \tag{20}$$

The relative phase is given by

$$e^{i(\theta_\downarrow - \theta_\uparrow)} = \frac{\mu^2 - r^2 e^{2i\varphi}}{\sqrt{(r^2 + \mu^2)^2 - 4\mu^2 r^2 \cos^2\varphi}} \tag{21}$$

and is singular at the two vortex cores $(\pm x_m, 0)$. Writing $(x, y) = (\pm x_m + \delta x, \delta y)$, a first-order expansion gives $\theta_\downarrow - \theta_\uparrow = \delta\varphi + \pi$ around $(x_m, 0)$ and $\theta_\downarrow - \theta_\uparrow = \delta\varphi$ around $(-x_m, 0)$, where $\delta\varphi = \arctan(\delta y/\delta x)$ is the local polar angle. When circling around each vortex core, the accumulated relative phase is 2π. Similarly, in the large distance limit $r \gg x_m$, the relative phase is $\theta_\downarrow - \theta_\uparrow = 2\varphi + \pi$ and a full loop around the two vortices generates a total phase change of 4π. This is slightly different from the usual meron pair situation [29], where the relative phase reaches a constant value at large

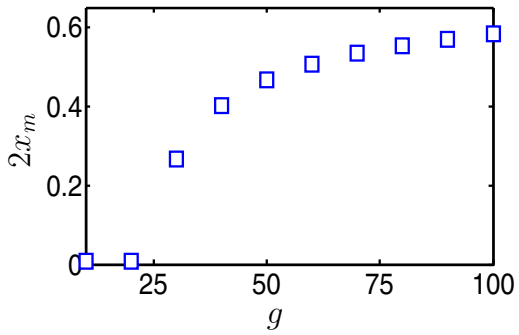

FIG. 7. (Color online) The size $2x_m$ of the meron pair, in units of the harmonic length $a_{ho} = \sqrt{\hbar/M\omega}$, as a function of g for $\Omega = 4$. The system exhibits a second-order phase transition at $g \approx 20$ between a ground state with topological properties similar to the $m = 0$ single-particle state and a meron pair with two opposite and off-centered vortices.

distance, which corresponds to a spin texture pointing in a fixed direction. In the present case, $(S_x, S_y) \approx (-\cos 2\varphi, -\sin 2\varphi)$. This difference explains why, in the present situation, the phase jumps happen on each outer side of the meron pair and not in between the two vortices; see Fig. 5(b). Apart from this, the GP ground state properties are similar to those of the meron pair already studied in a double-layer quantum Hall system [29,42].

By fitting our numerical data with ansatz Eq. (17), we have determined the parameters λ and α as a function of Ω and g. The results are shown in Fig. 7 for $\Omega = 4$. One can clearly see a phase transition happening at $g \approx 20$. Below, the GP ground state exhibits topological properties similar to the $m = 0$ single-particle state. Above, the GP ground state describes a meron pair with two off-centered and opposite vortices. It means that the energy cost to separate and shift away the vortex cores is less than the interaction energy. Above the transition point, the value of λ increases with g, which means that the size $2x_m$ of the meron pair increases. Finally, from the pseudospin point of view, the transition occurs between a uniformly vanishing $S_z(\mathbf{r})$ component and a well-defined structure $S_z(\mathbf{r})$. Therefore we expect the spin susceptibility along axis z to diverge at the transition and the phase transition is second order.

C. Phase diagram

Our previous analysis at strong and weak couplings have identified three topologically distinct ground states: the $m = 1$ vortex (also known as the Mermin-Ho vortex), the $m = 0$ vortex-antivortex, and the meron pair. A natural question to address next is then the phase diagram of the system in the (Ω, g) parameter plane. To this end, we have performed a numerical minimization of Eq. (11) for some particular values of Ω and g. Our results are summarized in Fig. 8 and suggest the existence of a tricritical point (Ω^*, g^*) where the three phases meet. As can be seen, the system always enters the meron pair phase at sufficiently strong interaction. For $\Omega < \Omega^*$, the system starts in the Mermin-Ho phase at low interactions and then, by increasing g, undergoes a first-order transition directly to the meron pair phase. Instead, for $\Omega^* < \Omega < \Omega_c$, one finds first a first-order transition between the Mermin-Ho phase

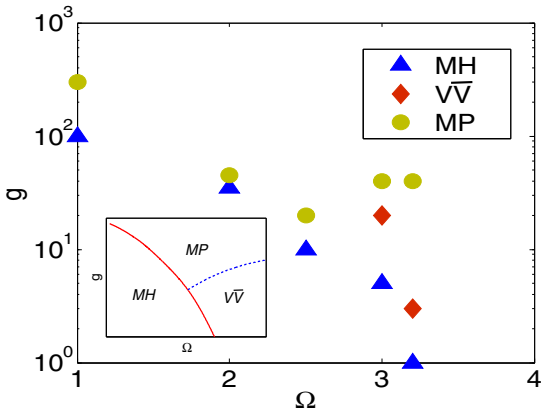

FIG. 8. (Color online) The topology of the ground states obtained at some particular values of Ω and g. Triangles: Mermin-Ho vortex (MH); full circles: meron pair (MP); diamonds: $m = 0$ vortex-antivortex ($V\overline{V}$). Our results suggest the existence of a tricritical point where the three phases meet. The inset shows a qualitative sketch of the phase diagram that we infer from our results. The transition from the MH phase to the MP and $V\overline{V}$ phases are first-order (solid line). The transition from the $V\overline{V}$ phase to the MP phase is second-order (dashed line).

and the $m = 0$ vortex-antivortex phase, then followed by a second-order transition between the $m = 0$ vortex-antivortex phase and the meron pair phase. For $\Omega > \Omega_c$, the system starts in the $m = 0$ vortex-antivortex phase and undergoes a second-order phase transition to the meron pair phase.

From an experimental point of view, the effective 2D interaction strength is given by $g_{2D} = \sqrt{8\pi} a_S / l_z$, where l_z is the harmonic length of the transverse confinement and a_S is the three-dimensional (3D) scattering length. In the case of the ^{87}Rb, the value of a_S is 5.2 nm and a strong transverse trap corresponds typically to $l_z \approx 0.25\ \mu m$, such that $g_{2D} \approx 0.1$. Therefore, with $N = 1000$ atoms in the trap, which is within experimental reach, one readily obtains an effective interaction strength $g_{2D} \times N = 100$.

IV. CONCLUSION

In this paper we have proposed an experimental scheme leading to nontrivial spin textures in the interacting ground state of a two-component spinor condensate. We have studied its phase diagram and identified three possible phases. At low enough coupling parameter Ω and interaction strength g, the ground state has the topology of a Mermin-Ho vortex. By increasing g at fixed Ω, this Mermin-Ho phase undergoes a first-order transition either to a meron pair phase or to a vortex-antivortex phase depending on the value of Ω. The vortex-antivortex and the meron pair phases are separated by a second-order transition line. A possible extension of the work is to study the excitations of the system and their topological properties. Finally, from an experimental point of view, $F = 1$ spinor condensates have also an effective spin-spin interaction $g_2 \mathbf{S}^2/2$. This interaction term breaks the $SU(2)$ invariance and converts a pair of bosons in the $|m_F = -1\rangle$ and $|m_F = +1\rangle$ spin states into a pair of bosons in the $|m_F = 0\rangle$ spin state. In the present situation, these collision processes correspond

to losses. In the case of ^{87}Rb, fortunately $g_2 \ll g$ and one should be able to observe the Mermin-Ho vortex and the meron pair before the effect of spin-spin interaction sets in. An alternative would be to lift the energy of the $|m_F = 0\rangle$ spin state and suppress the detrimental pair conversion processes by rendering them energetically less favorable.

ACKNOWLEDGMENTS

The Centre for Quantum Technologies is a Research Centre of Excellence funded by the Ministry of Education and National Research Foundation of Singapore.

APPENDIX

This Appendix contains the derivation of the effective atom-light coupling Hamiltonian (1).

The atom-light coupling Hamiltonian $H_{\rm AL}$ of the Λ scheme (see Fig. 1) reads

$$\begin{pmatrix} E_e & \Omega_1^* \cos(\omega_1 t) & \Omega_2^* \cos(\omega_2 t) \\ \Omega_1 \cos(\omega_1 t) & E_{-1} & 0 \\ \Omega_2 \cos(\omega_2 t) & 0 & E_1 \end{pmatrix}. \tag{A1}$$

The energies of the atomic levels are denoted by E_1, E_{-1}, and E_e, respectively. The Rabi frequencies for the electric-dipole transition at the laser frequencies ω_1 and ω_2 are Ω_1 and Ω_2.

It is convenient to transform the atomic states into the rotating frame via the unitary transformation

$$U(t) = \begin{pmatrix} \exp(-i\eta_e t) & 0 & 0 \\ 0 & \exp(-i\eta_{-1} t) & 0 \\ 0 & 0 & \exp(-i\eta_1 t) \end{pmatrix}, \tag{A2}$$

with $\eta_e = (E_1 + E_{-1} + \omega_1 + \omega_2)/2$, $\eta_{-1} = (E_1 + E_{-1} + \omega_2 - \omega_1)/2$, $\eta_1 = (E_1 + E_{-1} + \omega_1 - \omega_2)/2$.

The rotating wave approximation consists in removing the terms oscillating at frequencies $2\omega_{1,2}$ in the Hamiltonian $H(t) = U^\dagger(t) H_{\rm AL} U(t)$, such that the effective (time independent) Hamiltonian now reads:

$$H_{\rm rwa} = \frac{1}{2} \begin{pmatrix} 2\Delta & \Omega_1^* & \Omega_2^* \\ \Omega_1 & -\delta & 0 \\ \Omega_2 & 0 & \delta \end{pmatrix}, \tag{A3}$$

where $\Delta = (2E_e - \omega_1 - \omega_2 - E_1 - E_{-1})/2$ is the one photon detuning and $\delta = E_1 - E_{-1} + \omega_2 - \omega_1$ is the two photon detuning.

The evolution of the Λ scheme, in the rotating frame, obeys the Schrödinger equation

$$i \frac{\partial}{\partial t} \Psi = H_{\rm rwa} \Psi \quad \text{with} \quad \Psi = \begin{pmatrix} c_e \\ c_{-1} \\ c_1 \end{pmatrix}. \tag{A4}$$

Typically, (i) the initial state is taken in the $m_F = \pm 1$ subspace, i.e, with a vanishing population in the excited state $|e\rangle$; (ii) the one photon detuning Δ is very large, i.e., $|\Delta| \gg |\Omega_1|, |\Omega_2|, |\delta|$. In this case, the coupling with the excited state can be treated as a small perturbation for the evolution of the state in the $m_F = \pm 1$ subspace. More precisely, one can show that it results in a extremely slow evolution of the population in the excited state, which, at first order, amounts to writing

$$\frac{\partial}{\partial t} c_e = -\frac{i}{2} (\Omega_1^* c_{-1} + \Omega_2^* c_1 + 2\Delta c_e) = 0. \tag{A5}$$

We can therefore express c_e as a linear combination of c_{-1} and c_1, and thereby eliminate c_e in the evolution of the state, giving rise to the following effective Hamiltonian for the evolution of the Zeeman sublevels $m_F = \pm 1$:

$$-\frac{1}{4\Delta} \begin{pmatrix} 2\delta\Delta + |\Omega_1|^2 & \Omega_2 \Omega_1^* \\ \Omega_1 \Omega_2^* & -2\delta\Delta + |\Omega_2|^2 \end{pmatrix}. \tag{A6}$$

[1] M. Lewenstein, A. Sanpera, and V. Ahufinger, *Ultracold Atoms in Optical Lattices: Simulating Quantum Many-Body Systems* (Oxford University Press, Oxford, 2012).

[2] M. Lewenstein *et al.*, Adv. Phys. **56**, 243 (2007).

[3] I. Bloch, J. Dalibard, and W. Zwerger, Rev. Mod. Phys. **80**, 885 (2008).

[4] W. Ketterle and M. W. Zwierlein, in *Ultra-cold Fermi Gases*, Proceedings of the International School of Physics Enrico Fermi, Varenna, 20-30 June 2006, Course CLXIV, edited by M. Inguscio, W. Ketterle, and C. Salomon (IOS Press, Amsterdam, 2007), p. 95.

[5] N. R. Cooper, Adv. Phys. **57**, 539 (2008).

[6] Y.-J. Lin, R. L. Compton, A. R. Perry, W. D. Phillips, J. V. Porto, and I. B. Spielman, Phys. Rev. Lett. **102**, 130401 (2009).

[7] Y.-J. Lin, R. L. Compton, K. Jiménez-García, J. V. Porto, and I. B. Spielman, Nature (London) **462**, 628 (2009).

[8] Y.-J. Lin, K. Jiménez-García, and I. B. Spielman, Nature (London) **471**, 83 (2011).

[9] P. Wang, Z.-Q. Yu, Z. Fu, J. Miao, L. Huang, S. Chai, H. Zhai, and J. Zhang, Phys. Rev. Lett. **109**, 095301 (2012).

[10] L. W. Cheuk, A. T. Sommer, Z. Hadzibabic, T. Yefsah, W. S. Bakr, and M. W. Zwierlein, Phys. Rev. Lett. **109**, 095302 (2012).

[11] J. Struck, C. Ölschläger, M. Weinberg, P. Hauke, J. Simonet, A. Eckardt, M. Lewenstein, K. Sengstock, and P. Windpassinger, Phys. Rev. Lett. **108**, 225304 (2012).

[12] K. Jiménez-García, L. J. LeBlanc, R. A. Williams, M. C. Beeler, A. R. Perry, and I. B. Spielman, Phys. Rev. Lett. **108**, 225303 (2012).

[13] J. Dalibard, F. Gerbier, G. Juzeliūnas, and P. Öhberg, Rev. Mod. Phys. **83**, 1523 (2011).

[14] N. R. Cooper, Phys. Rev. Lett. **106**, 175301 (2011).

[15] G. Juzeliūnas, I. B. Spielman, New J. Phys. **14**, 123022 (2012).

[16] N. Goldman, G. Juzeliūnas, P. Öhberg, and I. B. Spielman, Rep. Prog. Phys. **77**, 126401 (2014).

[17] M. W. Ray, E. Ruokokoski, S. Kandel, M. Möttönen, and D. S. Hall, Nature (London) **505**, 657 (2014).

[18] Y.-X. Hu, C. Miniatura, D. Wilkowski, and B. Grémaud, Phys. Rev. A **90**, 023601 (2014).

[19] S. L. Zhu, H. Fu, C. J. Wu, S. C. Zhang, and L. M. Duan, Phys. Rev. Lett. **97**, 240401 (2006).
[20] T. D. Stanescu, B. Anderson, and V. Galitski, Phys. Rev. A **78**, 023616 (2008).
[21] R. Barnett, G. R. Boyd, and V. Galitski, Phys. Rev. Lett. **109**, 235308 (2012).
[22] V. Pietilä and M. Möttönen, Phys. Rev. Lett. **102**, 080403 (2009).
[23] N. Goldman, D. F. Urban, and D. Bercioux, Phys. Rev. A **83**, 063601 (2011).
[24] W. S. Cole, S. Zhang, A. Paramekanti, and N. Trivedi, Phys. Rev. Lett. **109**, 085302 (2012).
[25] D. Cocks, P. P. Orth, S. Rachel, M. Buchhold, K. Le Hur, and W. Hofstetter, Phys. Rev. Lett. **109**, 205303 (2012), and references therein.
[26] J. Minar and B. Grémaud, Phys. Rev. B **88**, 235130 (2013).
[27] L. S. Leslie, A. Hansen, K. C. Wright, B. M. Deutsch, and N. P. Bigelow, Phys. Rev. Lett. **103**, 250401 (2009).
[28] H. Zhai, W. Q. Chen, Z. Xu, and L. Chang, Phys. Rev. A **68**, 043602 (2003).
[29] K. Kasamatsu, M. Tsubota, and M. Ueda, Phys. Rev. Lett. **93**, 250406 (2004).
[30] K. Kasamatsu, M. Tsubota, and M. Ueda, Int. J. Mod. Phys. B. **19**, 1835 (2005).
[31] N. D Mermin and T.-L. Ho, Phys. Rev. Lett. **36**, 594 (1976).
[32] M. O. Scully and M. S. Zubairy, *Quantum Optics* (Cambridge University Press, Cambridge, UK, 1997).
[33] E. Brion, L. H. Pedersen, and K. Molmer, J. Phys. A **40**, 1033 (2007).
[34] K. C. Wright, L. S. Leslie, and N. P. Bigelow, Phys. Rev. A **78**, 053412 (2008).
[35] Kishore T. Kapale and Jonathan P. Dowling, Phys. Rev. Lett. **95**, 173601 (2005).
[36] Rina Kanamoto, Ewan M. Wright, and Pierre Meystre, Phys. Rev. A **75**, 063623 (2007).
[37] K.-P. Marzlin, W. Zhang, and B. C. Sanders, Phys. Rev. A **62**, 013602 (2000).
[38] R. Rajaraman, *Solitons and Instantons: An Introduction to Solitons and Instantons in Quantum Field Theory* (North-Holland, Amsterdam, 1982).
[39] K. Kasamatsu, M. Tsubota, and M. Ueda, Phys. Rev. A. **71**, 043611 (2005).
[40] T. Morinari, Phys. Rev. B **72**, 104502 (2005).
[41] J. Sinova, S. M. Girvin, T. Jungwirth, and K. Moon, Phys. Rev. B **61**, 2749 (2000).
[42] S. M. Girvin, in *The Quantum Hall Effect: Novel Excitations and Broken Symmetries*, Les Houches Lectures Notes, in Topological Aspects of Low Dimensional Systems, edited by A. Comtet, T. Jolicoeur, S. Ouvry, and F. David (Springer-Verlag, Berlin/Les Editions de Physique, Les Ulis, 2000).